

# COHERENT MOTIONS IN WINDBREAK FLOW

Y. ZHUANG<sup>1</sup> and J. D. WILSON<sup>2</sup>

<sup>1</sup>*Environmental Science Branch, AECL Research, Whiteshell, MB, Canada*

<sup>2</sup>*University of Alberta, Edmonton, AB, Canada*

(Received in final form 10 December, 1993)

**Abstract.** Experimental data on windbreak flows have been analysed, using several statistical methods. Our analysis demonstrates that coherent structures exist in the mixing region of a porous windbreak (50% porosity) flow, and are largely responsible for the momentum transport that re-accelerates the leeward flow. A comparison between windbreak flow and laboratory turbulent mixing layers suggests that the dominant structures in these two flows are similar. Some previous numerical and experimental results are interpreted in light of the coherent structures and the self-similar property in the mixing region of a windbreak flow.

## 1. Introduction

A windbreak, e.g., a fence, represents a simple example of a two-dimensional bluff obstacle. The flow behind the fence, influenced strongly by the aerodynamic interaction between the fence and the upstream wind field (the fence exerts a form drag force\* on the wind field), is characterized by strong velocity and pressure gradients in both horizontal and vertical directions (Plate, 1971; Bradley and Mulhearn, 1983).

Intuitively, a windbreak flow is likely to be a flow where coherent motions play an important role. However, ensemble-average turbulence models, which ignore the existence of coherent motions, have had some success in describing windbreak flows: for example, Wilson (1985) showed that the mean wind and some second-order statistics of a windbreak flow can be simulated reasonably well with a second-order closure model. It is curiosity about coherent structures and their possible role in windbreak flow that has resulted in this study.

All previous studies of such flows concerned ensemble-averaged properties, such as the attenuation of mean wind and turbulence by fences. Plate (1971) reviewed several aerodynamic aspects of a solid windbreak flow and demonstrated its complexity by dividing the flow into seven regions, each having different aerodynamic factors acting on it. In particular, Plate used a control volume to analyse alongwind momentum loss in the flow over a fence, and proposed a theoretical model relating windbreak drag to the leeward mean velocity field. Based on velocity and pressure measurements from wind tunnel experiments, and the analytical flow models, Plate concluded that “the effectiveness of a shelter is determined not only by its

\* Defined as  $D = 0.5C_d\rho HU_n^2$ , where  $C_d$  is the drag coefficient,  $\rho$  the air density and  $U_n$  the approaching wind speed at fence height  $H$ .

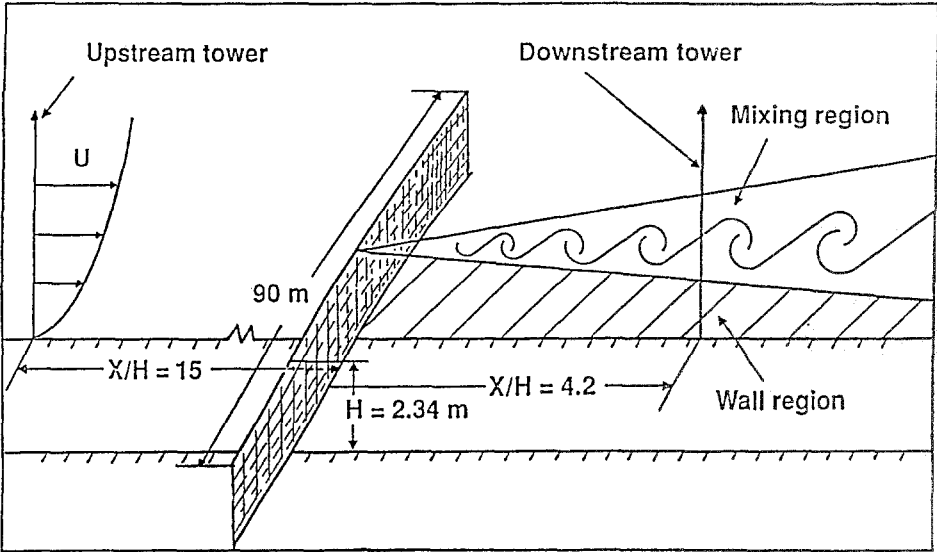


Fig. 1. A schematic picture of a typical experiment set up at Ellerslie. The wall region is bounded by the ground and a line extending from the top of the fence to the downstream point  $x = 15H$ .

total drag but also by the distribution of the drag generated momentum defect in the sheltered area”.

Using wind directions and fluctuations observed with a rotating vane, Baltaxe (1967) showed clearly that in the lee of fences, large-scale flow patterns existed, which varied with porosity of the fences, and disappeared when the porosity was larger than 25%. Raine and Stevenson (1977) demonstrated domination of the downstream flow by the fence-top generated turbulence, using measurements of turbulence intensity and spectra of the alongwind velocity downstream of the fences. Mulhearn and Bradley (1977) found, in their wind tunnel experiment, that the mean flow and momentum transport downstream of porous fences are very sensitive to the incident wind direction. A number of other factors, such as terrain roughness and the approaching wind profile, can also influence the downstream turbulence field (Plate, 1971).

Although it seems to have been generally accepted in previous studies that fence-top generated large-scale motions could be important in downstream flow, especially in the case of a solid fence, no reported study has discussed the detailed momentum transport processes associated with them, or explicitly taken into account their effects on downstream flow development. We feel that some of the experimental observations may be better understood from the instantaneous and structural points of view. It is with the large-scale structure in the downstream mixing region (Figure 1), and its role on downstream flow development, that the present study is concerned.

Experimental data from earlier authors (Mulhearn and Bradley, 1977; Bradley and Mulhearn, 1983), and from our own experiments, will be used. By examining the long-time turbulence statistics and the instantaneous flow structure, we shall show that coherent structures exist, and make a substantial contribution to momentum transport in the mixing region of a windbreak (50% porosity) flow. A comparison between windbreak flows and the laboratory turbulent mixing layer (Brown and Roshko, 1974) will demonstrate that the momentum transport achieved by the dominant structures in these two flows is similar, although a windbreak flow is more complex because of the unsteadiness (on long time scales) of the wind speed in the atmosphere, and the presence of the ground. Such a comparison suggests that, as in the turbulent mixing layer, the windbreak flow is self-similar in the mixing region, i.e., "motions at different sections differ only in velocity and length scales, and are dynamically similar in these aspects of controlling mean velocity and Reynolds stress" (Townsend, 1976).

We believe that coherent motions in the mixing region of a windbreak flow have a major influence on important aspects of the flow, such as intermittent flow reversal (observed behind dense windbreaks; Baltaxe, 1967), and the rate of downstream flow recovery. Wilson's (1985) numerical simulation and some previous field observations of windbreak flow will be discussed in light of the self-similar property and the observed coherent motions.

## 2. The Ellerslie experiment and data analysis

Our experiment was conducted at Ellerslie, Alberta, in the summer of 1989. A plastic fence (90 m long and 2.34 m high) was erected in an open field (Figure 1). The porosity of the fence was 50%, and its resistance coefficient ( $k_r = \Delta P / \rho U^2$ ), measured in a wind tunnel, was 1.66. The upstream fetch of uniform and level terrain was about 1 km. The surface was covered by long grass of about 30 cm. A log-law fit to an upstream wind profile measured under near neutral stratification yielded a surface roughness,  $z_0 \approx 0.1$  m.

The instrumentation included two 3-dimensional sonic anemometers (Applied Tech. Inc., 25-cm path length), two 1-dimensional sonic anemometers (Campbell Sci. Corp., 10 cm path length) and five cup anemometers. Using the sonic anemometers, time series of ( $u, v, w$ ) were sampled at 20 Hz, at points both upstream and downstream (mostly in the mixing region). In some cases the cup anemometers were mounted on the upstream tower to measure the approaching mean wind profile  $U(z)$ . In other cases, the mean wind profiles and turbulent fluctuations ( $u, v, w$ ) were measured simultaneously at the downstream tower. Data acquisition was accomplished by an analogue-to-digital converter coupled to a personal computer.

Since the heat flux was not measured, the Monin-Obukhov length, listed in Table I, was estimated using the flux-gradient relationships (Dyer, 1974) from the upstream mean wind profiles and weather conditions recorded nearby at the

TABLE I  
Long time statistics of windbreak flow in the Ellerslie experiments.

(a) Upstream measurements ( $X/H = -1.5$ $Z/H = 0.7$ )												
Run (duration)	$\sigma_u^2$	$Sk_u$	Kurt <sub>u</sub>	$\sigma_w^2$	$Sk_w$	Kurt <sub>w</sub>	$-\overline{uw}$	$-\overline{uw}/k$	$U_{5.5}$	$\sigma_w/u_*$	$\beta^*(\sigma_B)$ (*)	L (m)
1 (30 min)	1.1	0.3	3.2	0.2	0.1	3.6	0.16	0.14	6.2	1.12	26 (12)	102
2 (30 min)	0.42	0.18	2.5	0.06	0.05	4.12	0.04	0.1	3.1	1.22	17 (15)	-1
3 (10 min)	0.84	0.45	2.16	0.21	0.19	3.8	0.08	0.17	5.5	1.15	20 (16)	166
4 (20 min)	0.47	0.28	3.37	0.16	0.87	5.0	0.05	0.14	4.2	1.41	16 (11)	-2
5 (15 min)	0.34	0.24	3.51	0.12	0.14	4.41	0.06	0.13	3.1	1.55	?	-42
6 (30 min)	0.38	0.1	2.95	0.08	0.25	4.45		0.17	3.2	1.15	1 (20)	-1
Ave.		0.27	3.11		0.27	4.23		0.14				

\*  $\beta$  is the incident angle, which is zero when the wind is perpendicular to the fence.

(b) Downstream measurements (mixing and/or wall regions*)											
Run (duration)	$\sigma_u^2$	$Sk_u$	Kurt <sub>u</sub>	$\sigma_w^2$	$Sk_w$	Kurt <sub>w</sub>	$-\overline{uw}$	$-\overline{uw}/k$	$U_{5.5}$	Location	L (m)
1* (30 min)	0.21	0.13	3.40	0.11	-0.34	5.3	-0.02	<0	6.2	$X/H = 2.1$	$Z/H = 0.7$
2* (30 min)	0.06	0.18	3.24	0.04	-0.41	4.7	-0.06	<0	3.1	$X/H = 2.1$	$Z/H = 0.7$
4 (20 min)	0.2	0.34	3.89	0.15	-0.84	4.6	0.06	0.24	4.2	$X/H = 4.2$	$Z/H = 0.7$
5 (15 min)	0.25	0.34	3.19	0.07	-0.13	3.70	0.04	0.18	3.1	$X/H = 4.2$	$Z/H = 0.7$
6 (30 min)	0.18	0.8	3.70	0.11	-0.84	5.42	0.06	0.28	3.2	$X/H = 4.2$	$Z/H = 0.7$
7* (30 min)	0.89	0.83	3.98	0.47	-0.51	3.60	0.31	0.31	5.6	$X/H = 4.2$	$Z/H = 1.1$
7* (30 min)	0.22	0.10	4.20	0.10	-0.57	6.30	0.13	0.13	5.6	$X/H = 4.2$	$Z/H = 0.36$

\* Denotes observation in the wall region, which is bounded by the ground and a line extending from the top of the fence to the point  $x = 1.5H$ . The turbulence in the wall region is assumed to be close to equilibrium, i.e., turbulent energy production locally balances dissipation.

# The incident angle and its standard deviation for run 7 and 3° and 10°, respectively.

Edmonton International Airport. A total of 15 hours of data were collected under different atmospheric stability conditions. The long path length of the three-dimensional sonics filtered high frequency turbulent fluctuations, but these have no relevance to the present study of large-scale turbulence. To check the quality of the data, the mean horizontal velocity  $\sqrt{u^2 + v^2}$  according to the sonic anemometer(s) was compared with that of the cup anemometer(s) at the same location(s). We accepted the sonic data provided that the discrepancy was less than 10%. To minimize the influence of unsteadiness in wind direction on the data analysis, only the data collected under “steady” wind conditions, characterized by a small standard deviation of the wind direction ( $\sigma_\beta \leq 20^\circ$ ), have been selected (Table I).

### 2.1. LONG-TIME STATISTICS REVEALING ORGANIZATION AND GUSTINESS BEHIND A WINDBREAK

To examine the role of coherent motion in a windbreak flow, we have assumed that if the postulated structures exist, and have persistent and important impact on the flow, their effect should be seen not only in the instantaneous flow field, but also in the long-time statistics.

Table I lists some upstream and downstream turbulence statistics. Most runs included simultaneous measurements by sonic anemometers upstream and downstream. The ratio of the momentum flux ( $-\overline{uw}$ ) to the turbulent kinetic energy ( $k$ ),  $-\overline{uw}/k$ , measures the effectiveness of the turbulence in terms of momentum transport (Townsend, 1976). Upstream, on average,  $-\overline{uw}/k = 0.14$ , which is consistent with the value measured by Högström (1990) in the atmospheric surface layer, while in the downstream mixing region, this ratio is considerably larger. The variations of  $-\overline{uw}/k$  upstream are theoretically due to changes in atmospheric stability and boundary-layer depth. The variations downstream are attributed to variations in the incident wind direction, sensor location, and atmospheric stability, etc. Also notable in Table I is the significant difference between the skewness ( $Sk_w$ ) of the vertical velocities upstream and downstream.  $Sk_w$  is generally positive upstream, which agrees with previous observations for the atmospheric surface layer (e.g., Hunt *et al.*, 1988). However, large negative values of  $Sk_w$  were seen in most of the downstream observations, indicating strong sweeping motions (or gusts). It should be mentioned that since most of the runs lasted more than 15 minutes, during which time wind conditions varied, the effect of changing wind direction was averaged into the quantities in Table I.

Figures 2(a,b) show turbulence spectra of the fluctuating alongwind component ( $u$ ) and the momentum flux ( $-uw$ ), calculated for run 4, upstream and in the downstream mixing region. Upstream, the  $u$  spectrum peaks at considerably lower frequency than the  $-uw$  co-spectrum, which is consistent with the study by Kaimal *et al.* (1972). Downstream, the peak of the  $u$ -spectrum has moved to higher frequency, which agrees with a previous observation by Ogawa and Diosey (1980); and the peaks in the  $u$  and  $-uw$  spectra are much closer together downstream

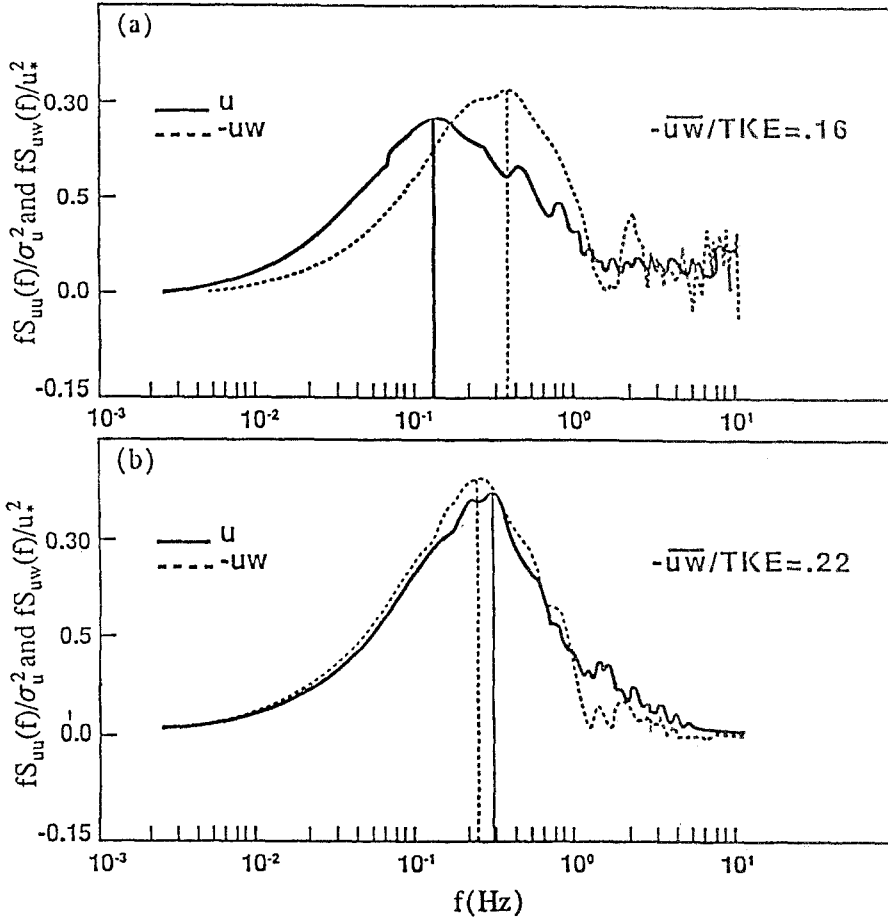


Fig. 2. Alongwind velocity and Reynolds stress spectra of the windbreak flow (a) upstream and (b) downstream mixing region, respectively. The data were measured at height  $z/H = 0.71$  during run 4. The mean wind speed at the upstream measurement height was  $2.44 \text{ m s}^{-1}$ .

than upstream. It is obvious from Figure 2(a) that upstream, some of the low-frequency content of the  $u$ -component does not contribute to momentum transport, although it does contribute substantially to the turbulent kinetic energy. Therefore, upstream, the Reynolds stress and turbulent kinetic energy may not be “carried by” the same “eddies” (Townsend, 1978). This agrees with the notion that there is a considerable amount of “inactive” motion (Högström, 1990) in the atmospheric surface layer. However in the downstream mixing region, the turbulent alongwind fluctuations are fully involved in momentum transport, resulting in the increased value of  $-\overline{uw}/k$  seen in Table I. In the atmospheric surface layer, spectra are greatly influenced by the unsteadiness of the advecting wind, in addition to the “phase scrambling” (Yule, 1980) of the eddies themselves; thus, no further attempt to infer the eddy structures has been based on spectral analysis.

The effective momentum transport seen in the long-time statistics and in the spectral characteristics shown above is presumably caused by increased organization and gustiness in the downstream flow. To reveal the coherent motion, conditional sampling and statistical methods will be used in the following sections, to extract (any) coherent motion from the measured velocity time series, and to reveal its role in the momentum transport process. We shall not be able to show the spatial characteristics of the coherent motion because of the very limited data available, but the temporal character will be described. Since runs 4 and 7 (Table I) were measured when wind conditions were relatively steady, they have been selected for analyzing upstream and downstream flows, respectively.

## 2.2. QUADRANT ANALYSIS

Quadrant analysis (Willmarth and Lu, 1974) is a method to sort momentum transport into sweep ( $u > 0$ ,  $w < 0$ ), ejection ( $u < 0$ ,  $w > 0$ ), inward interaction ( $u < 0$ ,  $w < 0$ ) and outward interaction ( $u > 0$ ,  $w > 0$ ) events. By doing so, and progressively filtering out smaller events ( $|uw| < \text{threshold value}$ ), one may identify large intermittent events that make a strong contribution to the momentum transport. Here quadrant analysis is used to study the structure of the Reynolds stress  $-\overline{uw}$ , from the instantaneous  $u$  and  $w$  signals measured in run 4 of our experiments.

Upstream and downstream structures of the Reynolds stress obtained using the quadrant analysis are shown in Figures 3. Upstream, the transport process is relatively symmetric, i.e., sweeps and ejections contribute equally and positively to the Reynolds stress, and inward and outward interactions contribute equally and negatively to the Reynolds stress. But downstream, the Reynolds stress is clearly dominated by sweeps. At large values of the hole size,  $H_0$ , when one selects lower frequency events with large Reynolds stress, this dominance becomes dramatic. For example, at  $H_0 = 10$ , the Reynolds stress is essentially produced by the sweep event alone, and represents about 37% of the total Reynolds stress. Furthermore, that 37% of the total Reynolds stress was found to be produced in less than 5% of the total sample time! The strong sweep motions transfer momentum excess, produced by the strong wind shear above the fence, from upper levels to lower levels, and result in the large negative skewness of the vertical velocity seen in Table I. The pattern of the downstream Reynolds stress structure changes little with atmospheric stability conditions. This agrees with Seginer (1974), who found that atmospheric stability has a minimal effect in the near-fence region, where, in our view, the windbreak-induced large-scale motions dominate the thermal effect.

## 2.3. CONDITIONAL SAMPLING

To investigate the velocity structures that dominate the Reynolds stress in the downstream flow, the VITA (Variable - Interval Time Averaging) technique (Blackwelder and Kaplan, 1976) will be used to identify "events". The VITA

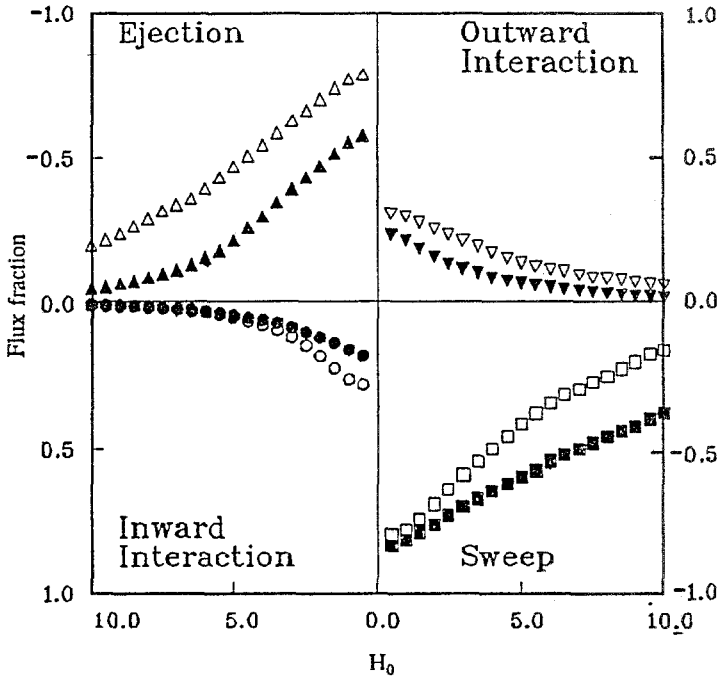


Fig. 3. Conditionally sampled structure of the Reynolds stress. Stress fraction in each quadrant versus hole size  $H_0$  in upstream and downstream mixing region (shaded symbols). At  $H_0 = 0$ , i.e., all scales contribute to the Reynolds stress, the stress fractions sum to  $-1$ . As  $H_0$  increases, the “small” scale turbulence has been filtered out to the hole region. The stress fraction is defined as

$$S_{i,H_0} = \frac{(uw)_{i,H_0}}{|uw|},$$

where the subscript  $i$  refers to quadrant number, and  $(uw)_{i,H_0}$  is the conditional average flux in  $i$ th quadrant at hole size  $H_0$ .

technique is based on the simple concept that peaks in the short-time variance signal correspond to dramatic events. The short-time variance is defined as

$$\text{VAR}(t, T) = \frac{1}{T} \int_{t-T/2}^{t+T/2} x^2(s) ds - \left\{ \frac{1}{T} \int_{t-T/2}^{t+T/2} x(s) ds \right\}^2, \quad (1)$$

where  $x$  is a signal fluctuation with its long-term mean subtracted out. When  $T$  becomes large, the second term on the right-hand side of (1) tends to zero, and the long-time variance,  $\sigma_x^2$ , is obtained. There is a close relation between the integration time  $T$  and the time scale of  $x$  contributing to the short-time variance. For example, Schols (1984) found that Equation (1) works roughly as a low-pass filter, accepting frequencies below  $1/T$ . On the basis of a visual inspection of the measured velocity time series, it is found that the violent coherent motions usually last between 3 to 5 s. Since we are interested in the velocity structure of the violent

sweep motions selected with the quadrant analysis in Section 2.2, which have a relatively long time scale,  $T = 5$  s was chosen for the present study.

Instead of using the  $u$  velocity component as the event selector (as was the case in most previous applications), the momentum flux,  $-uw$ , was used as the controlling VITA variable. This is because, in a laboratory study of a turbulent mixing layer, Bradshaw (1966) found that maximum instantaneous momentum flux occurs during the large-eddy pairing process; so events selected by VITA using  $-uw$  triggering should correlate well with the large-scale motions.

The events (velocities in a time domain centered at the instant when the maximum of the short-time variance occurs) are selected when VITA exceeds the long-time averaged variance of  $-\overline{uw}$ . The time domain was chosen to be 6 s so that it will cover a complete period of most of the selected events. One hundred events were selected for each upstream and downstream location. The selected events contributed about 70% of the momentum flux in about 50% of the total time, for both upstream and downstream locations.

The major difference between previous applications of the VITA technique and the present study is in the stage of ensemble averaging. It is important to remember that the selected events may contain contributions from a number of scales. Most previous authors formed an arithmetical average of the selected events. But in the atmospheric surface layer, owing to the unsteadiness of the wind, the ensemble-averaged events could be a blurred superposition of the embedded structures, and show no order (Narasimha and Kailas, 1987).

To examine the VITA-selected turbulent events, we have used the method of Proper Orthogonal Decomposition (Lumley, 1967, 1981), which is a statistical method widely used to sort from a large set of experimental observations a subset of linear combinations of coherent patterns contributing maximally to the observed variance. It has been successfully applied in this context to identify coherent motions in turbulent jets (Glauser *et al.*, 1985) and in the wall region of a turbulent boundary layer (Aubry *et al.*, 1988). Here, because of the limited data available, only a simple version of this theory is applied: only the temporal variation of the data will be considered. Details of this theory can be found in Aubry (1991) and the references listed therein, but a very brief description follows.

#### 2.4. PROPER ORTHOGONAL DECOMPOSITION

Suppose  $f_1(t), f_2(t), \dots, f_N(t)$  are  $N$  realizations (or events) of a fluctuating signal, each of which can be either a single variable or a composite of variables, sampled periodically at time interval,  $\Delta t = (T_2 - T_1)/M$ , within the closed domain  $[T_1, T_2]$ . By requiring a function  $\phi(t)$ , defined on the domain  $[T_1, T_2]$ , to resemble in a statistical sense the dominant structure embedded in these realizations, one obtains for  $\phi(t)$  the prescription

$$\sum_{m=0}^M R(t_m, t_k) \phi(t_m) = \lambda \phi(t_k), \quad (2)$$

where  $R(t_m, t_k)$  is the two-time covariance function formed from the  $N$  realizations  $f$ , which is a  $(M + 1) \times (M + 1)$  matrix, and  $\lambda$  is the eigenvalue. Equation (2) is the well-known problem of determining eigenvalues and eigenvectors of a matrix  $R(t_m, t_k)$ . Solving this eigenvalue problem (IMSL, 1989), one finds a set of eigenvalues  $(\lambda_1, \dots, \lambda_N)$ , ordered such that  $\lambda_1 > \lambda_2 > \dots > \lambda_N > 0$ , and a set of corresponding orthogonal functions  $(\phi_1(t), \dots, \phi_N(t))$ .

Each event can then be reconstructed from the orthogonal functions

$$f_i(t) = \sum_{n=1}^N \alpha_{in} \phi_n(t), \quad (3a)$$

where

$$\alpha_{in} = \sum_{m=0}^M f_i(t_m) \phi_n(t_m), \quad (3b)$$

with different coefficients,  $\alpha_{in}$ , for each different event.

For flows having a high degree of organization, this decomposition has been found very effective in the sense that the first few orthogonal functions will effectively retain most of the information in the velocity covariance of the selected events.

To implement the Proper Orthogonal Decomposition to obtain the orthogonal functions, the selected events were arithmetically averaged every 0.1 s, i.e., low-pass filtered, and used to calculate the two-time covariance function

$$R(t_m, t_k) = \frac{1}{N} \sum_{i=1}^N \mathbf{F}_i^T \mathbf{F}_i, \quad (3c)$$

where  $(^T)$  denotes a transpose and  $\mathbf{F}_i$  is a  $1 \times 120$  matrix:  $[u_i(t_1), w_i(t_1), \dots, u_i(t_{60}), w_i(t_{60})]$ ; so the covariance,  $R(t_m, t_k)$ , contains the variances of  $u$  and  $w$  components, as well as the covariance of  $u$  and  $w$ .

To be consistent with the objective of investigating the velocity structures that dominate the Reynolds stress, we weighted the selected events with their respective values of the Reynolds stress  $W_{uw}(i)$  averaged over the domain  $[T_1, T_2]$ , when calculating  $R(t_m, t_k)$ :

$$R(t_m, t_k) = \frac{1}{N} \sum_{i=1}^N W_{uw}(i) \mathbf{F}_i^T \mathbf{F}_i. \quad (3d)$$

Thus, the resulting eigenvectors calculated from (2) emphasize the velocity events, not only effectively retaining information in velocity covariance but also making the largest contributions to  $-uw$ . Such weighted orthogonal functions have been calculated and used by Marht and Frank (1988) to explain the transport character of the intermittent turbulence at the top of a strongly stratified surface inversion layer.

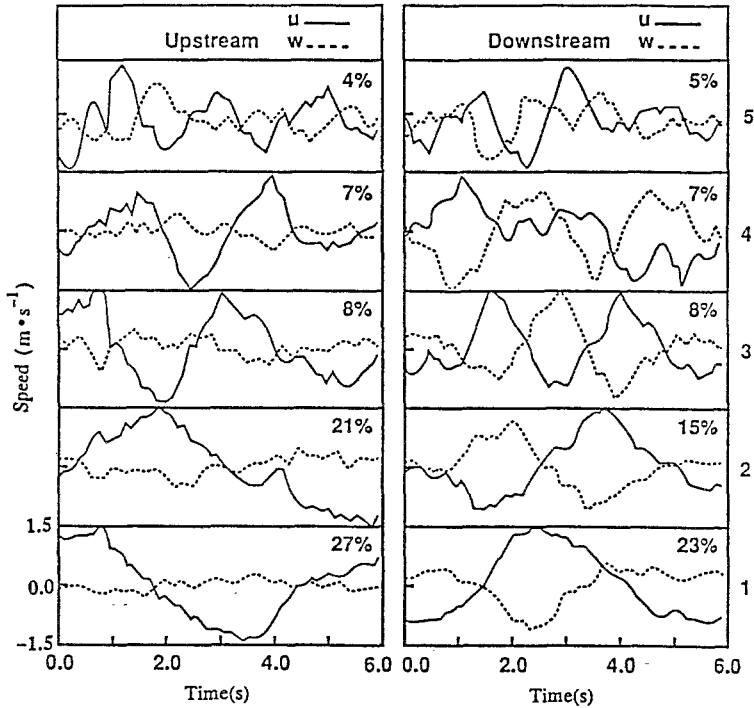


Fig. 4. First five orthogonal functions obtained by P.O.D. of velocity time series observed upstream and downstream of a fence. The % are the fraction each velocity structure contributes to the total variance of the VITA-selected events. The velocity scale applies to all five structures.

Figure 4 shows the five most important orthogonal functions extracted from events contributing strongly to the Reynolds stress, for the upstream and downstream turbulence. These five velocity structures contribute more than 50% of the velocity variance of the selected 100 ( $N$ ) events, and represent, in decreasing order, the largest scale motions. Upstream, the vertical velocity components are not well correlated with the alongwind components, and have a small amplitude, implying that most momentum transport happens when there is a strong alongwind fluctuation and a weak downdraft. This is expected in the undisturbed atmospheric surface layer, where horizontal motions dominate. But downstream,  $u$  and  $w$  have about the same amplitude, and are better correlated within the selected events, implying an effective momentum transport mechanism in the downstream turbulence.

The analysis so far suggests that indeed there are strong coherent motions in the mixing region of a windbreak flow. However, our data are too limited to discuss further the coherent motions, their spatial structure, and their role in determining the evolution of a windbreak flow. For this, we shall rely on earlier windbreak experiments. In addition, it is noted that the strongly coherent down-

stream  $u$  and  $w$  events resemble the velocity measurements from a laboratory turbulent mixing layer, where the primary structures are the transverse vortices that have strong vertical motions (Latigo, 1979). Thus, if a resemblance (both mean flow and turbulence) between windbreak flow and the turbulent mixing layer can be established, the well known properties of the turbulent mixing layer will shed light on what we may expect to ultimately be revealed as the vortical nature of windbreak flow.

### 3. A Resemblance between Windbreak Flow and the Turbulent Mixing Layer

A turbulent mixing layer is formed by the sudden interaction of two parallel streams having initially (i.e., at the point of conjunction) distinct and uniform velocities  $U_1$  and  $U_2$ . Although the simplest statistical theory of the turbulent mixing layer based on an eddy viscosity is well known (Schlichting, 1968), study of the coherent structures in the turbulent mixing layer has been an active academic problem (Latigo, 1979; Liu, 1989), and has played an important role in research aimed at better understanding of turbulent shear flow. The essential feature of a turbulent mixing layer is the presence of spanwise coherent large-scale vortices, which are believed to be a manifestation of hydrodynamic instability (Ho and Huerre, 1984). Following this primary instability, secondary instabilities introduce three-dimensionality into the flow. Roshko (1980) concluded that "development of a mixing layer is largely determined by the primary spanwise vortices and the streamwise counter rotating vortex pairs. The Reynolds stress and the growth of the layer are controlled mainly by the primary vortices while the secondary set provides internal mixing and possibly modifies the stress."

For a solid fence, Plate (1971) demonstrated that the flow near the separation streamline (i.e., a line passing close to the tip of the fence, and dividing the downstream flow into "high" and "low" velocity regions) can be well described by the simplest theory of the turbulent mixing layer, which involves the assumption of an eddy viscosity,  $k_\nu$ , varying linearly with downstream distance  $x$ :

$$k_\nu = \frac{x}{4\sigma^2} (U_1 - U_2). \quad (4)$$

Here  $U_1$  and  $U_2$  are the flow velocities above and below the windbreak, and  $\sigma$  is an empirical constant.

In the case of a porous fence, we would expect that the upper part of the flow field ( $z > H$ ), which is distorted (relative to the upstream flow) owing to the drag on the fence, would have characteristics similar to the upper-layer flow of a solid fence, but with less severe distortion. Theoretical and wind tunnel studies reviewed by Laws and Livesey (1978) have shown that a uniform screen blocking a confined flow always tends to make the downstream wind more uniform. By varying the resistant coefficient  $k_r$ , the downstream mean velocity profile can be controlled.

In addition, with increasing porosity, the mean flow recirculation zone right behind a windbreak weakens (Baltaxe, 1967) and the flow in the mixing region will not be affected by ground as strongly as in the case of a solid fence. Thus, it is reasonable to assume that in the mixing region of a porous windbreak, the flow has the characteristics of the flow that results if an upper flow with initially uniform velocity,  $U_1$ , is joined to a lower flow of velocity  $U_2$ .

Experiments (Finnigan and Bradley, 1985) show that there is a small downward curvature in the mean downstream streamline, which is caused by the pressure gradient between ground and the upper layer free stream, i.e., the “Coanda” effect (Plate, 1971). Plate pointed out that the Coanda effect is in part responsible for the recovery of the wind profile to its upstream equilibrium condition in solid windbreak flows, but suggested that this effect is probably small for a porous fence. We thus neglect it in the following discussions.

To test the hypothesized resemblance of windbreak flow to turbulent mixing-layer flow, we have used the experimental data of Bradley and Mulhearn (1983), who designed a windbreak experiment in the atmospheric surface layer to verify a theory proposed by Counihan *et al.* (1974), for the wake behind a fence in a boundary layer. The fence was 1.2 m in height, with a porosity of 50% and a resistance coefficient  $k_r = 2$ . Using drag plates, and cup and sonic anemometers, velocity and shear stress profiles were measured at various locations downstream of the fence, under near neutral stability conditions. The downstream patterns of velocity and shear stress were found independent of the upstream wind velocity over the range 5–10 m/s. Figure 5 shows the mean profiles upstream and downstream of a windbreak, reproduced from Bradley and Mulhearn. Immediately behind the windbreak ( $x/H = 0.8$ ), the wind profile is relatively uniform below windbreak height. The wind profiles in the mixing region ( $x/H = 8.3, 12.5, 16.7$ ) have been plotted in Figure 6 using mixing-layer scaling. The solid line in Figure 6 is the solution for the velocity profile in a turbulent mixing layer, namely

$$U = \frac{U_1 + U_2}{2} \left\{ 1 + \frac{U_1 - U_2}{U_1 + U_2} \operatorname{erf}(\eta) \right\}, \quad (5)$$

where  $\eta = \sigma z/x$  is the similarity variable for the mixing layer. The empirical constant  $\sigma$  was specified as 14.5, as suggested by Plate (1971) for both solid and porous fences; erf is the error function. For our purposes, the speeds  $U_1$  and  $U_2$  have been normalized by the velocity at 4 m. Then  $U_1 = 1.0$  while from the wind profile at  $x/H = 0.8$ ,  $U_2 = 0.4$ . From Equation (5) the momentum flux  $\tau$  is calculated as

$$\tau = \rho k_v \frac{\partial U}{\partial Z}, \quad (6)$$

which is presented in Figure 7 along with Bradley and Mulhearn’s experimental data at two downstream locations.

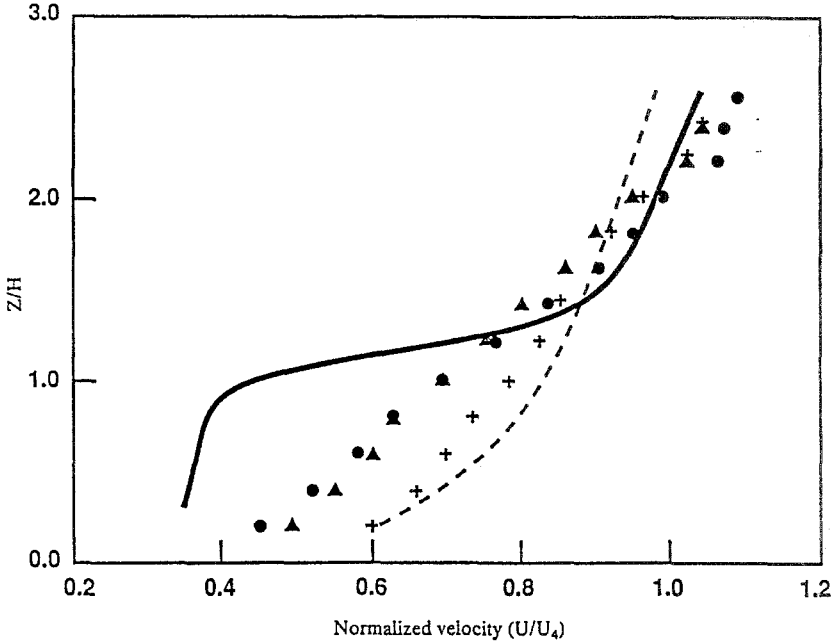


Fig. 5. Mean wind profiles measured under near neutral conditions, reproduced from Bradley and Mulhearn's (1983) experiment. The wind profiles are normalized by the velocity at 4 m. The dashed line denotes the upstream wind profile; —  $X/H = 0.8$ ; ●  $X/H = 8.3$ ; ▲  $X/H = 12.5$ ; +  $X/H = 16.7$ .

Since the data were averaged over many different runs, scatter around the theoretical curves could be partly due to variations in atmospheric stability and incoming wind directions. Qualitative agreement between the experimental data and the theoretical calculations in Figures 6 and 7 indicates that in the mixing region of the windbreak flow, both mean flow and second-order statistics follow (qualitatively) the turbulent mixing-layer scaling.

Further evidence of the resemblance between windbreak flow and the turbulent mixing layer can be extracted from Mulhearn and Bradley's (1977) experiment, in which the authors examined the sensitivity of windbreak flow to incident wind direction in a wind tunnel. Mulhearn and Bradley found that with a decrease of incidence angle in the approaching wind direction (i.e., when the upstream wind is more nearly perpendicular to the fence), the downstream mean wind profiles tend to decrease mostly near and below the windbreak height (i.e., the velocity difference  $U_1 - U_2$  becomes larger), whereas the momentum fluxes tend to increase strongly, especially at heights greater than half of a fence-height. That is, the larger the difference between velocities at upper and lower levels of a windbreak, the stronger the downstream momentum transport. This phenomenon is also found in the turbulent mixing layer. From Equations (5) and (6), we obtain

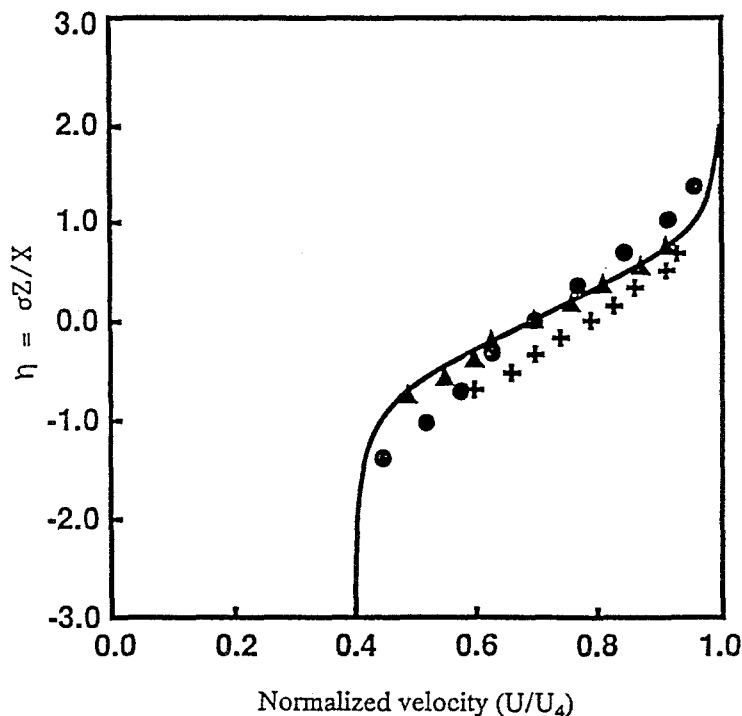


Fig. 6. Theoretical and experimental mean wind profiles in the mixing region of the windbreak, expressed in mixing-layer scaling. — Equation (5); Experiment (Bradley and Mulhearn, 1983): ●  $X/H = 8.3$ ; ▲  $X/H = 12.5$ ; +  $X/H = 16.7$ .

$$\tau = \frac{1}{2} \rho \kappa_v (U_1 - U_2) \frac{\partial}{\partial z} \operatorname{erf}(\eta). \quad (7)$$

Thus, a mixing layer with a larger velocity difference,  $U_1 - U_2$ , will transport momentum more effectively.

It seems plausible, from the above comparisons, that the dominant flow structure in the mixing region of a windbreak is similar to a classical turbulent mixing layer. Having established this connection, we shall try to explain some of the interesting phenomena of windbreak flows.

#### 4. Discussion and Conclusion

Why do turbulence models, such as the eddy viscosity closure and the second-order closure, which do not explicitly account for the occurrence of coherent motions, lead to fairly reasonable prediction of the mean flow in what we now know to be an organized windbreak flow (Wilson, 1985)? To address this question, let us recall some experimental evidence on the turbulent mixing layer. Following extensive turbulence measurements in a plane mixing layer, Wygnanski and Fiedler

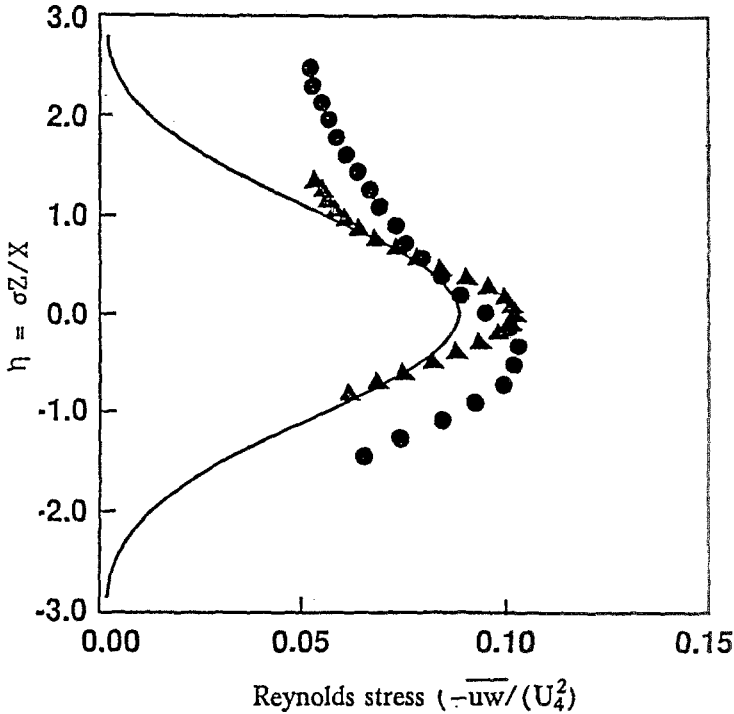


Fig. 7. Theoretical and experimental Reynolds stress profiles in the mixing region of the windbreak, expressed in mixing-layer scaling. — Equation (6); Experiment (Bradley and Mulhearn, 1983): ●  $X/H = 8.3$ ; ▲  $X/H = 15.0$ .

(1970) claimed that “in spite of the complexity of the flow, the simple concepts of eddy viscosity and eddy diffusivity appear to be valid within the turbulent zone.” Shih (1984) successfully simulated a turbulent mixing layer using a second-order model. His success, as Lumley (1985) points out, is partly because, in a self-similar flow, all scales of the turbulence respond quickly to changes in the mean flow field, so the coherent motions transport momentum in much the same way as the “fine grain” turbulence does, and can be described by the gradient transport theory. The self-similar properties of a turbulent mixing layer have been demonstrated by Spencer and Jones (1971) in a wind tunnel experiment where the fluctuating velocities were found to closely follow the mean velocity in attaining a similar distribution. In view of the resemblance between windbreak flows and the turbulent mixing layer, the successful numerical simulation of a windbreak flow by Wilson (1985) based on the Reynolds equations is not surprising.

From laboratory experiments we know that the thickness of a turbulent mixing layer is linearly proportional to the normalized velocity difference,  $(U_1 - U_2)/(U_1 + U_2)$  (Browand and Troutt, 1985). On the other hand, from the aerodynamic point of view, the normalized velocity difference between upper and lower levels of a windbreak flow (immediately behind the fence) is determined by

parameters such as porosity, incident wind direction, etc. Observations (Raine and Stevenson, 1977) showed that the higher the porosity of the fence, the slower the rate of recovery to the upstream condition in the far wake. Since the mean wind profile downstream is shaped by the momentum transport, in light of what we have shown we can assert that the slow recovery is caused by the fact that with increasing porosity, the normalized velocity difference behind the fence decreases, and the large-scale coherent motions become less effective and need a longer distance to transport the alongwind momentum required to restore the wind profile to the equilibrium upstream condition. For the same reason, when the incident wind is oblique to the fence, the normalized velocity difference behind the fence is decreased, leading to the reduced momentum transport observed in a windbreak flow (Mulhearn and Bradley, 1977).

Finnigan and Bradley (1983) found that immediately behind a fence, the zone of enhanced turbulent kinetic energy (relative to upstream) covered a deeper vertical region than the zone of enhanced shear stress. Similar differences (although of lesser degree) can be seen in a turbulent mixing layer (Wynanski and Fiedler, 1970). The narrow zone of the enhanced stress may correspond to the pairing process of the coherent motions, that happens in the region of a large velocity gradient. The deeper zone of enhancement of turbulent kinetic energy could be due to the very large eddy (larger than the scale considered here) induced swirling "inactive" motions, which are particularly intense in a boundary layer with adverse pressure gradient ( $dp/dx > 0$ ) (Townsend, 1976), such as in the lee of a windbreak (Plate, 1971). "Inactive" motions contribute little to the Reynolds stress, but compose a significant part of the turbulent kinetic energy.

Since the drag coefficient of a windbreak,  $C_d$ , varies little with atmospheric stability, we do not expect the normalized velocity difference, and consequently the structure of momentum transport in the near wake of a windbreak, to change with atmospheric stability. This has been confirmed by our quadrant analysis, and by Seginer (1974). The changes in flow pattern in the far wake of a windbreak flow are however influenced by the local thermal structure, and can not be easily predicted.

In conclusion, we have shown that coherent motions occur in a porous windbreak flow, and argued that they resemble the vortices seen in a laboratory turbulent mixing layer. By virtue of their strong  $u - w$  correlation, the coherent motions are largely responsible for the momentum transport that reaccelerates the leeward flow. However, from the modelling point of view, the coherent motions in a windbreak flow do not pose great difficulties, because of the self-similar properties of the flow in the mixing region.

#### Acknowledgements

We appreciate the generosity of G. W. Thurtell of the University of Guelph for lending us his three-dimensional sonic anemometers. We are grateful to an

anonymous referee for many constructive comments on an earlier version of this manuscript. We thank our colleagues T. Flesch, B. Amiro and P. Davis for reviewing this manuscript. This work has been supported in part by the Natural Sciences and Engineering Research Council of Canada (NSERC) and the Atmospheric Environment of Service (AES) of Environment Canada.

### References

- Antonia, R. A.: 1981, 'Conditional Sampling in Turbulence Measurement', *Annu. Rev. Fluid Mech.* **13**, 131–56.
- Aubry, N.: 1991, 'On the Hidden Beauty of the Proper Orthogonal Decomposition', *Theoret. Comput. Fluid Dynamics* **2**, 339–352.
- Aubry, N., Holmes, P., Lumley, J. L., and Stone, E.: 1988, 'The Dynamics of Coherent Structures in the Wall Region of A Turbulent Boundary Layer', *J. Fluid Mech.* **192**, 115–173.
- Baltax, R.: 1967, 'Air Flow Patterns in the Lee of Model Windbreaks', *Archiv fur Meteorologie, Geophysik und Bioklimatologie, Series B: Allgemeine und biologische Klimatologie*, Band **15**, Heft 3, 26 pp.
- Blackwelder, R. F., and Kaplan, R. E.: 1976, 'On the Wall Structure of Turbulent Boundary Layer', *J. Fluid Mech.* **76**, 89–112.
- Bradley, L. F., and Mulhearn, P. J.: 1983, 'Development of Velocity and Shear Stress Distributions in the Wake of A Porous Shelter Fence', *J. Wind Eng. Ind. Aerodyn.* **15**, 145–156.
- Bradshaw, P.: 1966, 'The Effect of Initial Conditions on the Development of a Free Shear Layer', *J. Fluid Mech.* **26**, 225–236.
- Browand, F. K. and Troutt, T. R.: 1985, 'The Turbulent Mixing Layer: Geometry of Large Vortices', *J. Fluid Mech.* **158**, 489–509.
- Brown, L. G., and Roshko, A.: 1974, 'On the Density Effects and Large Structure in Turbulent Mixing Layer', *J. Fluid Mech.* **64**, 775–816.
- Counihan, J., Hunt, J. C. R. and Jackson, P. S.: 1974, 'Wakes Behind Two-Dimensional Surface Obstacles in Turbulent Boundary Layers', *J. Fluid Mech.* **64**, 529–563.
- Courant, R., and Hilbert, D.: 1953, *Methods of Mathematical Physics* **1**, Interscience, 561 pp.
- Dyer, A. J.: 1974, 'A Review of Flux-Profile Relations', *Boundary-Layer Meteorol.* **1**, 363–372.
- Finnigan, J. J., and Bradley, B. F.: 1983, 'The Turbulent Kinetic Energy Budget Behind A Porous Barrier: An Analysis in Streamline Coordinates', *J. Wind Eng. Ind. Aerodyn.* **15**, 157–168.
- Ho, C-M., and Huerre, P.: 1984, 'Perturbed Free Shear Layers', *Annu. Rev. Fluid Mech.* **16**, 365–424.
- Högström, U.: 1990, 'Analysis of Turbulence Structure in the Surface Layer with a Modified Similarity Formulation for Near Neutral Conditions', *J. Atmos. Sci.* **47**, 1949–1972.
- Hunt, J. C. R., Kaimal, J. C., and Gaynor, J. E.: 1988, 'Eddy Structure in the Convective Boundary Layer – New Measurements and New Concepts', *Q. J. R. Meteorol. Soc.* **114**, 827–858.
- IMSL, 1989: IMSL- Fortran Subroutines for Mathematical Applications, MALB-USM-PERFCT-EN8901–1.1.
- Kaimal, J. C., Wyngaard, J. C., Izumi, Y., and Cote, O. R.: 1972, 'Spectral Characteristics of Surface Layer Turbulence', *Quart. J. Roy. Meteorol. Soc.* **98**, 563–589.
- Latigo, Ben O.: 1979, 'Large-Scale Structure Interactions in a Two-Dimensional Turbulent Mixing Layer', Ph.D. Thesis, Dept. Aero-Space Engng., Univ. S. Calif., Los Angeles.
- Laws, E. M. and Livesey, J. L.: 1978, 'Flow Through Screens', *Ann. Rev. Fluid Mech.* **10**, 247–266.
- Liu, J. T. C.: 1989, 'Coherent Structures in Transitional and Turbulent Shear Flows', *Annu. Rev. Fluid Mech.* **21**, 283–315.
- Loeve, M.: 1955, *Probability Theory*, Van Nostrand, N.Y.
- Lumley, J. L.: 1967, 'The Structure of Inhomogeneous Turbulent Flows', in A. M. Yaglom and V. I. Tatarsky (eds.), *Atmospheric Turbulence and Radio Wave Propagation*, pp. 166–178.
- Lumley, J. L.: 1981, 'Coherent Structure in Turbulence', in R. E. Meyer (ed.), *Transition and Turbulence*, pp. 215–242. Academic Press, N.Y.

- Mahrt, L., and Frank, H.: 1988, 'Eigen Structure of Eddy Microfronts', *Tellus* **40A**, 107–119.
- Mulhearn, P. J., and Bradley, E. F.: 1977, 'Secondary Flows in the Lee of Porous Shelterbelts', *Boundary-Layer Meteorol.* **12**, 75–92.
- Narasimha, R., and Kailas, S. V.: 1987, 'Energy Events in the Atmospheric Boundary Layer', in H. U. Meier and P. Bradshaw (eds.), *Perspectives in Turbulence Studies*, Springer-Verlag, pp. 188–222.
- Ogawa, Y., and Diosey, P. G.: 1980, 'Surface Roughness and Thermal Stratification Effects on the Flow Behind a Two-Dimensional Fence II: A Wind Tunnel Study and Similarity Considerations', *Atmos. Environ.* **14**, 1309–1320.
- Plate, Erich J.: 1971, 'The Aerodynamics of Shelter Belts', *Agriculture Meteorol.* **8**, 203–222.
- Raine, J. K. and Stevenson, D. C.: 1977, 'Wind Protection by Model Fences in A Simulated Atmospheric Boundary Layer', *J. Ind Aerodyn.* **2**, 159–180.
- Roshko, A.: 1980, 'The Plane Mixing Layer, Flow Visualization Results and Three-Dimensional Effects', in: J. Jimenez (ed.), *The Role of Coherent Structures in Modelling Turbulence and Mixing*. Lecture notes in Physics, Springer, Vol. 136, pp. 206–217.
- Schlichting, H.: 1968, *Boundary-Layer Theory*, McGraw Hill.
- Schols, J. L. J.: 1984, 'The Detection and Measurement of Turbulent Structures in the Atmospheric Surface Layer', *Boundary-Layer Meteorol.* **29**, 39–58.
- Seginer, Ido: 1974, 'Atmospheric-Stability Effect on Windbreak Shelter and Drag', *Boundary-Layer Meteorol.* **8**, 383–400.
- Seginer, Ido: 1975, 'Flow Around a Windbreak in Oblique Wind', *Boundary-Layer Meteorol.* **9**, 133–141.
- Shil, T.-H.: 1984, 'Second Order Modelling of Scalar Turbulent Flow', Ph.D. thesis, Cornell University, Ithaca, N.Y.
- Sirovich, L.: 1987, 'Turbulence and Dynamics of Coherent Structures: I, II, III', *Quart. Appl. Math.* **5**, 561–590.
- Spencer, B. U., and Jones, B. G.: 1971, 'Statistical Investigation of Pressure and Velocity Fields in the Turbulent Two-Stream Mixing Layer', *AIAA Paper*, No. 71-613.
- Townsend, A. A.: 1976, *The Structure of Turbulent Shear Flow*, Cambridge University Press, 429 pp, 2nd ed.
- Townsend, A. A.: 1978, 'Flow Patterns of Large Eddies in a Wake and in a Boundary Layer', *J. Fluid Mech.* **95**, 515–537.
- Willmarth, W. W., and Lu, S. S.: 1974, 'Structure of the Reynolds Stress and the Occurrence of Bursts in the Turbulent Boundary Layer', *Advances in Geophysics* **18A**, 287–314.
- Wilson, J. D.: 1985, 'Numerical Studies of Flow Through a Windbreak', *J. Wind Eng. and Indust. Aerodynamics.* **21**, 119–154.
- Wynanski, I., and Fiedler, H. E.: 1970, 'The Two-Dimensional Mixing Region', *J. Fluid Mech.* **41**, 327–361.
- Yule, A. J.: 1980, 'Phase Scrambling Effects and Turbulence Data Analysis', in L. J. S. Bradbury et al. (eds.), *Turbulent Shear Flow II*, Springer-Verlag, Berlin, pp. 263–281.